Supporting Information for

Shape-Controlled Deterministic Assembly of Nanowires

Yunlong Zhao[†], Jun Yao[†], Lin Xu[†,§], Max N. Mankin[†], Yinbo Zhu[⊥], Hengan Wu[⊥], Liqiang Mai[§], Qingjie Zhang[§] & Charles M. Lieber[*,†,‡]

[†]Department of Chemistry and Chemical Biology, and [‡]Harvard John A. Paulson School of Engineering and Applied Sciences, Harvard University, Cambridge, Massachusetts 02138, United States

[§]State Key Laboratory of Advanced Technology for Materials Synthesis and Processing, Wuhan University of Technology, Wuhan 430070, China

[⊥]CAS Key Laboratory of Mechanical Behavior and Design of Materials, Department of Modern Mechanics, University of Science and Technology of China, Hefei, Anhui 230027, China

This file includes:

Materials and Methods

Nanowire synthesis. Silicon nanowires were synthesized using a gold (Au) nanoparticle-catalysed vapour-liquid-solid (VLS) process described previously.[1] Briefly, 10, 30 and 80 nm diameter Au nanoparticles (15703, 15706 and 15710, Ted Pella, Redding, CA) were dispersed on the SiO_2 surface of Si growth substrates (600 nm thermal SiO_2, Nova Electronic Materials, Flower Mound, TX). Nanowire growth was carried out at 430–455 °C. Specifically, the intrinsic nanowires were synthesized at a total pressure of 40 Torr with 2.5 standard cubic centimetres per minute (sccm) silane (SiH_4, 99.9999%, Voltaix, Branchburg, NJ) as the silicon reactant, 60 sccm hydrogen (H_2, 99.999%; Matheson, Basking Ridge, NJ) as the carrier gas. Growth temperatures of 435 °C, 450 °C, and 450 °C were used for diameters of 10, 30, and 80 nm, respectively. For the synthesis of p-type nanowires, additional 3.1 sccm diborane (B_2H_6, 100 p.p.m. in H_2, Voltaix, Branchburg, NJ) was introduced as the p-type dopant. Growth temperatures of 430 °C, 450 °C, and 450 °C were used for diameters of 10, 30, and 80 nm, respectively. Intrinsic nanowires were used for nanowire assembly and p-type nanowires were used for fabrication of bioprobe device arrays in this work. Typical growth times of 1–2 h yielded nanowires with average lengths of 40–80 μm.

Shape controlled assembly. A range of target substrates were used in our studies, including Si wafers (Nova Electronic Materials, Flower Mound, TX) with SiO_2, Si_3N_4, Au, nickel (Ni) and SU-8 polymer (SU-8 2000.5, Microchem, Inc., Westborough, MA) surface layers. The substrate surface layer was cleaned by rinsing in isopropanol (IPA, Cleanroom® MB, KMG Electronic Chemicals, Inc., Houston, TX) for 30 s followed by nitrogen drying. LOR 1A and diluted S1805 (1:2 (vol : vol) diluted in Thinner-P) (Microchem, Westborough, MA) for photolithography (PL)

or double layer polymethyl methacrylate (PMMA, 950-C2, Microchem, Westborough, MA) for electron beam lithography (EBL) was spin-coated, and PL or EBL was used to define arrays of trenches with thicknesses of ~260 nm and with shapes and widths as described in the main text. For trenches with thicknesses of ~20, ~50, ~130, and ~260 nm, diluted PMMA 950-A2 (1:1 (vol : vol) diluted in Anisole), PMMA 950-A2, PMMA 950-C2 and PMMA 950-A6 was spin-coated as resist, respectively. The minimum radii of curvature trench structures fabricated by PL and EBL were 1.5 μm and 200 nm, respectively. No additional surface modification followed exposure and development of these patterns.

Shape-controlled assembly of nanowires was carried out in a manner similar to shear-printing described elsewhere.[1-3] Briefly a target substrate patterned with an array of trenches was mounted onto a micromanipulator-controlled moveable stage, covered with mineral oil (330760, viscosity, v, $\approx$ 70 mPa•s, Sigma-Aldrich, St. Louis, MO), and then the nanowire growth substrate was brought into contact with the target substrate with controlled contact pressure (values in text). The target substrate was moved at a constant velocity of ~5 mm min^{-1} with respect to the fixed nanowire growth substrate, and then the growth substrate was removed and the target substrate rinsed with octane (98%, Sigma-Aldrich, St. Louis, MO) to remove the lubricant. The minimum radius of nanowire curvature achievable by this process was determined by using ca. 200 nm radii of curvature trenches fabricated by EBL for 80 and 30 nm diameter silicon nanowires. For 10 nm diameter silicon nanowires, 76 +/- 1.1 nm (mean +/- standard deviation) radius Au nanoparticles (15712, Ted Pella, Redding, CA; size statistics obtained from the vendor's characterization) were used as anchoring means. In this case, the Au nanoparticles were dispersed on SiO_2/Si substrate modified with poly-L-lysine (P8920, Sigma-Aldrich, St. Louis, MO), followed by deposition of ~10 nm thick Al_2O_3 film by atomic layer deposition

(ALD) at 150^{o}C (90 cycles). In addition, experiments were carried out by placing the nanowire growth substrate directly over the substrate with trenches, translating approximately 100–200 μm, and then removing the growth substrate and imaging the positions of the transferred nanowires with respect to the trenches; the data in Figure 2a was obtained in this manner.

TEM sample preparation and characterization. Arrays of U-shaped silicon nanowires with different radii of curvature were prepared for transmission electron microscopy (TEM) characterization by fixing the arms of the assembled wires between Au metal layers while leaving the suspended nanowire tips exposed for imaging. We introduced Au layers on both top and bottom of patterned PMMA for assembly as follows. (1) A Ni sacrificial layer (100 nm) was deposited on an oxidized silicon substrate by thermal evaporation (TE). (2) A square mesh gold ribbon network (100 nm) was defined on the Ni layer by EBL and TE. (3) Arrays of U-shaped 80 nm diameter silicon nanowires were patterned as described above such that the straight arms and U-tips were on top of the gold mesh and open areas, respectively. (4) PMMA under the straight arms of U-shaped nanowires was cross-linked by EBL using a dose of ~8,000 μC/cm^2. (5) A second Au mesh (100 nm thick) which was coincident in the x-y plane with the bottom mesh was defined on top of the cross-linked PMMA and deposited via TE. (6) The nickel sacrificial layer was etched in nickel etchant (TFB, Transene Company, Inc., Danvers, MA) for 1 h and then the free-standing arrays of U-shaped silicon nanowires embedded in the Au-mesh/PMMA/Au-mesh trilayer were transferred to a copper TEM grid (300 mesh Cu, Ted Pella, Redding, CA). TEM characterization (JEOL 2100, JEOL Ltd. or aberration-corrected Zeiss Libra MC TEM, Carl Zeiss AG) was carried out at a beam accelerating voltage of 200 kV. Fourier-filtered images

processed from the high-resolution TEM (HRTEM) images were used to characterize dislocations in the bent nanowires.

Strain release tests. Arrays of suspended U-shaped silicon nanowires were transferred to TEM grids as described above and introduced into a focused ion beam (FIB) instrument (dual ion/electron beam Zeiss NVision 40, Carl Zeiss AG). The FIB was used to cut one of the two suspended arms of a U-shaped nanowire (Ga^+ ions, 30 kV) while monitoring the nanowire release process *in situ* by SEM video-rate imaging (8 frames per second).

Raman spectroscopy characterization. Arrays of suspended U-shaped silicon nanowires with some nanowires cut by FIB in a free-standing mesh supported on a Cu TEM grid were placed on a glass slide. Straight nanowires that adhered in random positions on the PMMA surface (i.e., not bent during the assembly process) were also transferred and suspended in the same mesh for control measurements. Raman spectra were acquired with a LabRam Evolution Multiline Raman Spectrometer (Horiba, Kyoto, Japan) equipped with 1800 blaze/mm grating and a 100x microscope objective lens with numerical aperture (N.A.) of 0.95. A continuous-wave (CW) diode laser with a wavelength of 633 nm was used as incident light source and circularly polarized using a zero-order quarter waveplate optimized for 633 nm. The laser power was ~26 μW and the laser spot size was ~1.5 μm in diameter.

Finite element simulations of nanowire bending. A geometrically nonlinear finite element model was used to simulate the large deformations of nanowires under load. The modelling and simulations were carried out with commercial ANSYS 14.5 software. In our model, the nanowire

is considered as a linearly elastic cantilever beam with elastic modulus of 188 GPa and Poisson ratio of 0.3 characteristic of silicon.[4] The length and diameter of the cantilever beam are 20 μm and 80 nm, respectively. The in-plane forces generated during the experimental assembly process are expected to produce approximately uniform distributed bending loads, which are applied in the simulations; these uniform bending loads ranged from 0 to 20 nN/μm. The deformation of the nanowire under different loading is shown in Figure 2d. The corresponding load-dependent radii of curvature at the fixed end were calculated from the simulated results and are plotted in Figure 2e.

Bend-up nanowire probe arrays. Arrays of U-shaped silicon nanowires were used as building blocks to fabricate three-dimensional (3D) bend-up nanoprobe device arrays. Briefly, (1) a Ni sacrificial layer (100 nm) was defined by EBL and deposited on a silicon substrate (600 nm thermal SiO_2). (2) The substrate was coated with SU-8 resist (1:1 diluted SU-8R 2000.5 in cyclopentanone, Microchem, Inc., Westborough, MA), and then the bottom SU-8 support layer was defined by EBL. (3) After definition of the U-shaped PMMA trench arrays by EBL, U-shaped 10−80 nm diameter silicon nanowires were deterministically assembled in the trenches. (4) Source/drain metal contacts Cr/Pd/Cr (1.5/75/50 nm) were defined by EBL and TE. Typically, the source/drain contact separation was 1.5 μm in each probe, and the free end of the nanowire extended 2−6 μm from the source contact. (5) A top SU-8 (SU-8R 2000.5, Microchem, Inc., Westborough, MA) layer was subsequently defined by EBL to complete the passivation of the metal contacts/interconnects. (6) The nickel layer was etched (~1 h, TFB etchant, Transene Company, Inc., Danvers, MA) to yield the 3D bend-up probes. The individual nanowire probe devices were fabricated without registration to nanowires, since the patterns of bottom SU-8

passivation layer, contact electrodes and top SU-8 passivation layer, and *x*- and *y*- coordinates of U-shaped nanowires all precisely match the original trench pattern used for U-shape deterministic assembly; that is, the process follows a design-oriented fabrication approach.[5]

Device sensitivities were characterized by water-gate measurements in 1× phosphate buffered saline (PBS) with a Ag/AgCl reference electrode.[6-8] The nanowire device conductance values were measured with a DC bias of 0.5 V, and the current was converted to voltage with a current preamplifier (10^{-7} A/V, Model 1211, DL Instruments, Brooktondale, NY), and digitized at 20 kHz sampling rate (Axon Digi1440A, Molecular Devices). The sensitivity of our U-shaped silicon nanowires is 2.5 ± 2.0 μS/V. The sensitivity of our previous reported kinked silicon nanowires[6] is 8.5 ± 4.3 μS/V.

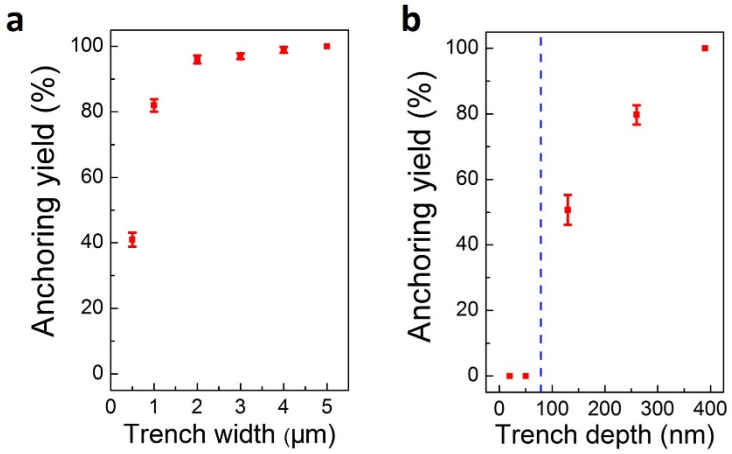

Figure S1. Dependence of nanowire anchoring yields on key trench dimensions. The nanowire anchoring yield versus trench (a) width and (b) depth. For (a), trench widths are 0.5, 1, 2, 3, 4, 5 μm and depth is fixed at 260 nm. For each data point, statistics is based on analysis of 210 sites randomly selected. For (b), trench depths are 20, 50, 130, 260, 390 nm and width is fixed at 3 μm. For each data point, statistics is based on analysis of 600 sites randomly selected. The blue vertical dashed line corresponds to the 80 nm diameter nanowires used in the measurements. These results indicate that trench width and depth can be used to optimize the anchoring yield of nanowires during assembly.

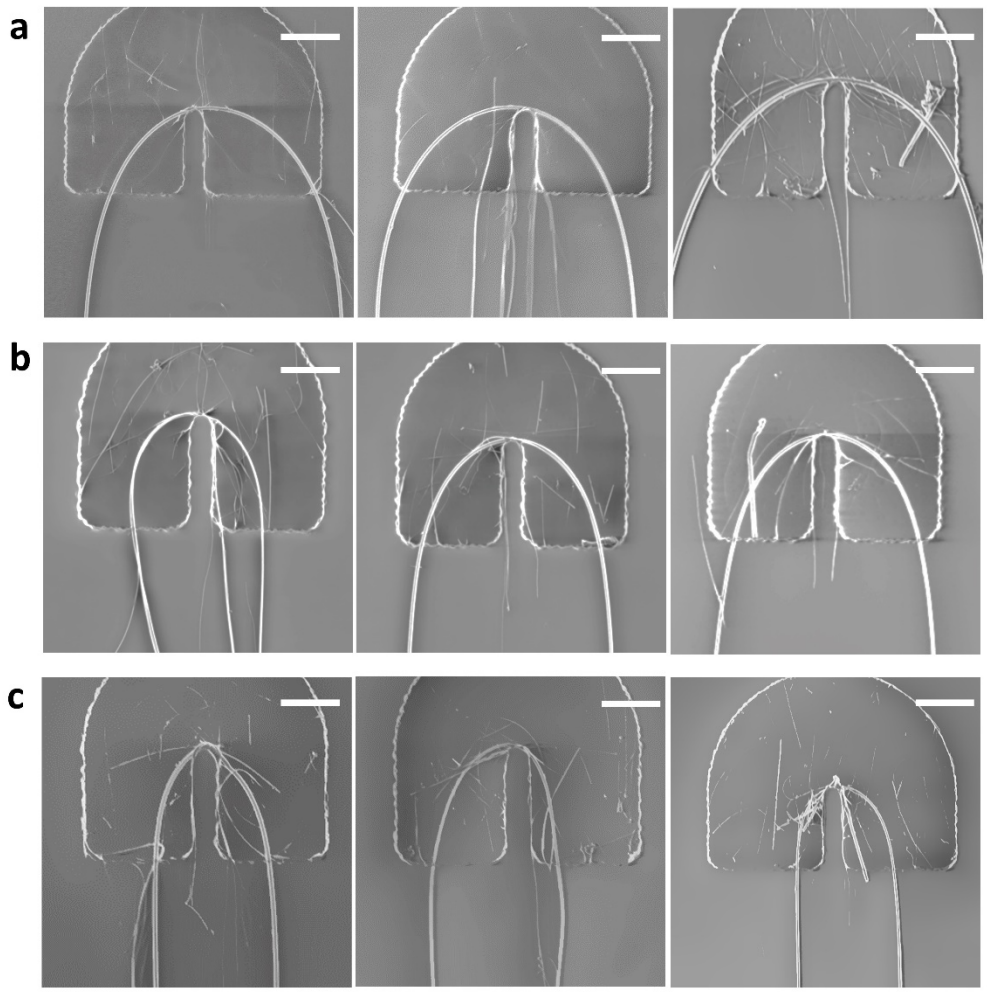

Figure S2. Dependence of nanowire bending curvature on contact pressure. Representative SEM images of 80 nm diameter silicon nanowires assembled with normal pressures of (**a**) 0.8, (**b**) 4.8 and (**c**) 7.2 N cm^{-2}. Scale bars all 1 μm. These results are consistent with increasing in-plane bending loads as the contact pressure is increased; that is, we find decreases in nanowire radius of curvature with increasing bending loads (simulation) or transfer normal pressures (experiments).

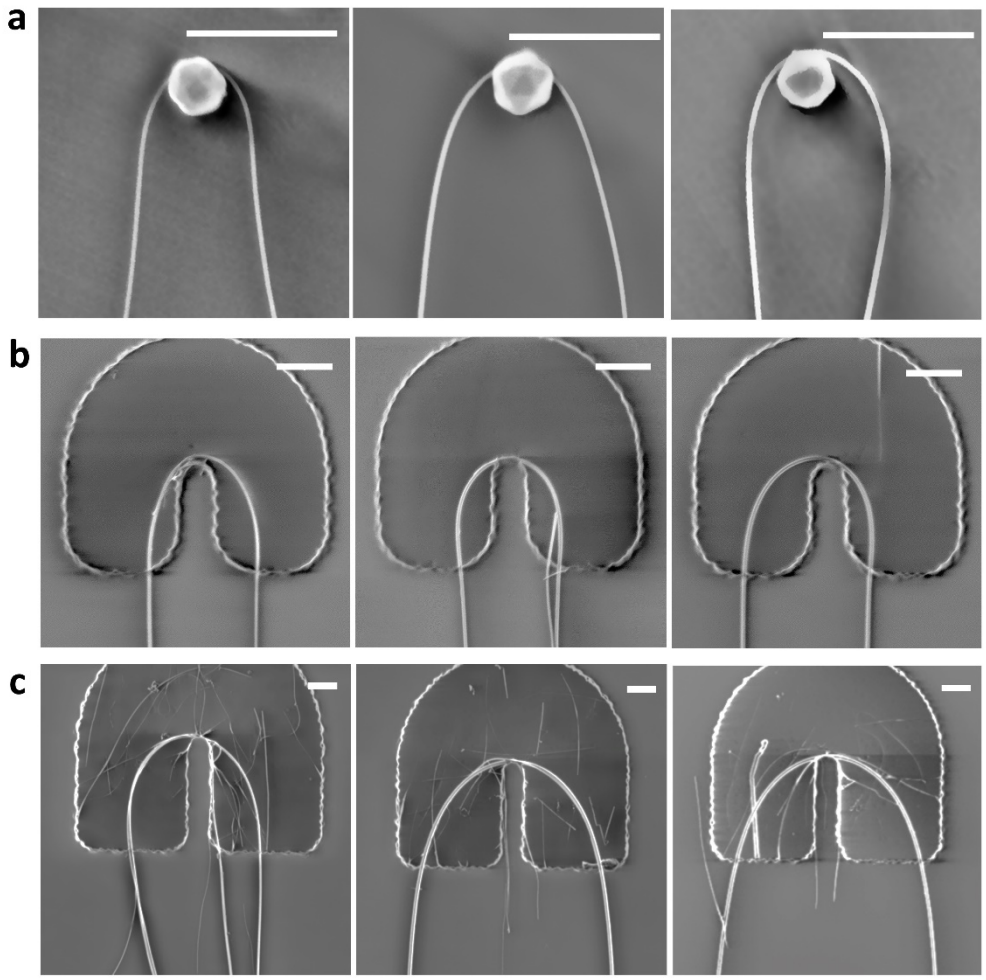

Figure S3. Dependence of nanowire bending curvature on nanowire diameter. Representative SEM images of silicon nanowires with different diameters assembled with normal pressures of 4.8 N cm^{-2}. **a**, 10 nm diameter nanowires anchored on Au particles (radii ~75 nm). **b**, 30 nm diameter nanowire anchored on trenches with depth of 130 nm, width of 1μm, and radii of inner curvature of 200 nm. **c**, 80 nm diameter nanowire anchored on trenches with depth of 260 nm, width of 3 μm, and radii of inner curvature of 200 nm. Scale bars, 500 nm.

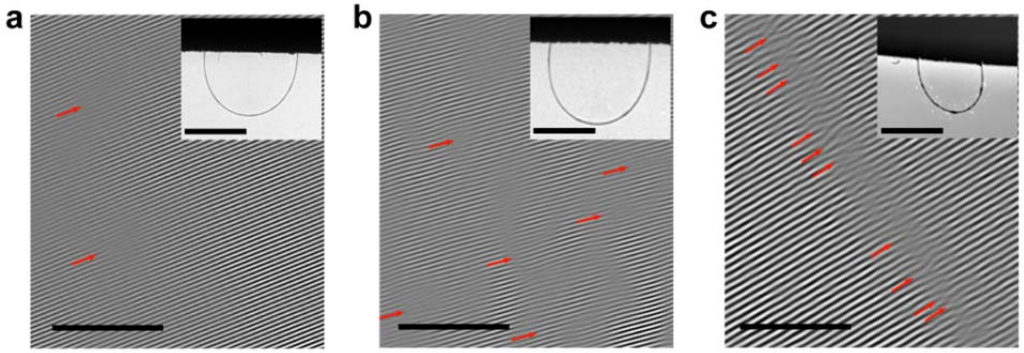

Figure S4. TEM images of U-shaped silicon nanowires. a-c, Fourier-filtered high resolution TEM images of the tips of assembled U-shaped nanowires (all nanowire diameters are 80 nm) with radii of curvature of 3.0, 1.5, and 0.8 μm in **a**, **b** and **c**, respectively. Red arrows indicate dislocations. Scale bars, 5 nm. Insets, low magnification TEM images of the U-shaped, suspended nanowires. Inset scale bars are 4, 2 and 2 μm in **a**, **b** and **c**, respectively. TEM analysis indicates that the overall dislocation density in the curved portions of the nanowires increases as the radius of curvature decreases.

Supplementary Video 1. SEM video recordings of the release process of a U-shaped silicon nanowire. The radius of curvature of the U-shaped nanowire (diameter = 80 nm) assembled on a copper TEM grid is 1.5 μm before cutting one arm with a FIB. After cutting the upper arm at the position indicated by the green arrow, the nanowire springs back to an almost straight configuration, suggesting that much of the strain introduced during U-shaped assembly of the nanowires is elastic.

Supplementary References

1. Yao, J.; Yan, H.; Lieber, C. M. *Nat. Nanotechnol*. **2013**, *8*, 329–335.
2. Yan, H.; Choe, H. S.; Nam, S. W.; Hu, Y.; Das, S.; Klemic, J. F.; Ellenbogen, J. C.; Lieber, C. M. *Nature* **2011**, *470*, 240–244.
3. Fan, Z.; Ho, J. C.; Jacobson, Z. A.; Yerushalmi, R.; Alley, R. L.; Razavi, H.; Javey, A. *Nano Lett.* **2008**, *8*, 20–25.
4. Stan, G.; Krylyuk, S.; Davydov, A. V.; Cook, R. F. *J. Mater. Res.* **2012**, *27*, 562–570.
5. Yao, J.; Yan, H.; Das, S.; Klemic, J. F.; Ellenbogen, J. C.; Lieber, C. M. *Proc. Natl. Acad. Sci. U. S. A.* **2014**, *111*, 2431–2435.
6. Qing, Q. Jiang, Z.; Xu, L.; Gao, R.; Mai, L.; Lieber, C. M. *Nat. Nanotechnol*. **2014**, *9*, 142–147.
7. Xu, L.; Jiang, Z.; Qing, Q.; Mai, L.; Zhang, Q.; Lieber, C. M. *Nano Lett.* **2013**, *13*, 746–751.
8. Xu, L.; Jiang, Z.; Mai, L.; Qing, Q. *Nano Lett.* **2014**, *14*, 3602–3607.